

PAPER • OPEN ACCESS

## Water-Assisted Co-Injection Molding of Non-Circular Tubes

To cite this article: T Q Kuang *et al* 2019 *IOP Conf. Ser.: Earth Environ. Sci.* **267** 042164

View the [article online](#) for updates and enhancements.

# Water-Assisted Co-Injection Molding of Non-Circular Tubes

T Q Kuang<sup>1</sup>, P Xu<sup>1</sup>, Q Feng<sup>1</sup> and L S Turng<sup>2</sup>

<sup>1</sup>School of Mechatronics & Vehical Engineering, East China Jiaotong University, Nanchang, China

<sup>2</sup>Department of Mechanical Engineering, University of Wisconsin–Madison, WI, USA

**Abstract.** Water-assisted co-injection molding (WACIM) is a complex and creative injection molding process. A three-dimensional model for WACIM was setup and a  $k - \omega$  turbulence model was adopted to deal with the turbulent flow of the water. The volume of fluid (VOF) method was used to track the moving interfaces of the skin–inner melt and the inner melt–water. Numerical simulations for the filling stage of WACIM parts with four types of cross-sections were carried out with the computational fluid dynamics (CFD) method. Experiments were conducted to verify the simulation results. The results of the experiments were in agreement with those of the simulations. The cross-section shape of the cavity had a significant effect on the penetrating area of the inner melt, while the shape of the water permeation eventually becomes round. The penetration area of the water increased in the flow direction, and the residual wall thicknesses of the inner melt downstream was thinner than the melt upstream.

## 1.Introduction

Water-assisted co-injection molding (WACIM), a new processing technology, was first developed to produce media ducts and multilayer hollow parts [1, 2]. WACIM can be considered a combined processing technology of water-assisted injection molding (WAIM) and co-injection molding (CIM) processes. WAIM is a process similar to gas-assisted injection molding, but presents a number of advantages including fast cooling, short cycle times, thin wall thicknesses, material savings, cost savings, no sink marks, smooth inner surfaces, and more uniform veins [3-5]. CIM can be used to manufacture parts with some special characteristics by combining different plastic materials, such as using the skin material to achieve required surface properties while using the core material to obtain demanded mechanical properties or to reduce cost [6, 7]. WACIM has the advantages of both WAIM and CIM. Moreover, it has a wider processing window [1]. Now WACIM technology is mainly used to produce automotive, household, and furniture items, highlighting a bright future for WACIM about market prospects.

The water-assisted co-injection molding process can be identified into two types: short-shot water-assisted co-injection molding (SS-WACIM) and full-shot water-assisted injection molding (FS-WACIM). In SS-WACIM, two different polymer melts are first sequentially injected and partially filled into the mold cavity, and a skin/core structure was formed, then finally water is injected into the core of the polymer melt. In FS-WACIM, first the polymer melts are fully filled into the mold cavity in sequence, and then high pressure water is injected to push the material into the overflow cavity.

L. Yan [8], T.-Q. Kuang [9], K. Zhang [10, 11], and G.-F. Zhou [12] investigated the influence of processing parameters, including melt temperature, water injection delay time, water pressure, water temperature, and mold temperature on the residual wall thickness of WACIM parts via numerical simulation. Most of their studies were focused on a simple tube with a circular cross-section, and the models used were two-dimensional axisymmetric models. While there is literature available on the cored



out shapes of water-assisted injection molded parts [13], no one has ever studied the penetration shapes of the inner melt and the water in WACIM parts with non-circular cross-sections.

The present report is devoted to studying the penetration sections of the inner melt and the water in WACIM of non-circular tubes by simulation technology and experimentation. A three-dimensional model for WACIM was set up and numerical simulations for the filling stage of WACIM parts with different cross-sections were carried out. The experiments were performed to verify the simulation results.

## 2. Model and Simulation

### 2.1 Mathematical Model

In order to predigest the flow process and facilitate the simulation, the following simplifications and assumptions have been made to WACIM based on the CFD method.

1. In the initial state, the skin melt (the melt first injected) filled the mold cavity evenly, and its injection process didn't affect the following penetration—that's the FS-WACIM.
2. The melt and the water were considered as incompressible fluids; Those properties such as density, heat capacity, and thermal conductivity were supposed constant.
3. The melt flow met a no-slip boundary; the body forces and surface tension were neglected.

Governing equations consisted of the continuity equation, motion equation, energy equation, constitutive equation, viscosity model, and volume fraction equation.

The continuity equation deals with the law of conservation of mass, expressed as

$$\frac{\partial \rho}{\partial t} + \frac{\partial}{\partial x_i} (\rho u_i) = 0 \quad (1)$$

The random nature of the turbulent flow must be taken into consideration in the motion equation for the high Reynolds number (high turbulence) of the injection of water. Reynolds stresses were introduced into the motion equation based on traditional injection molding. The Reynolds time-averaged motion equation is,

$$\frac{\partial}{\partial t} (\rho u_i) + \frac{\partial}{\partial x_j} (\rho u_i u_j) = \frac{\partial}{\partial x_j} \left[ \mu \left( \frac{\partial u_i}{\partial x_j} + \frac{\partial u_j}{\partial x_i} - \frac{2}{3} \delta_{ij} \frac{\partial u_l}{\partial x_l} \right) \right] - \frac{\partial p}{\partial x_i} + \frac{\partial}{\partial x_j} (-\rho \overline{u'_i u'_j}) \quad (2)$$

where the last item is the Reynolds stress.

The relationship between the Reynolds stress and the average velocity gradient can be expressed based on the Boussinesq eddy viscosity assumption as follows,

$$-\rho \overline{u'_i u'_j} = \mu_t \left( \frac{\partial u_i}{\partial x_j} + \frac{\partial u_j}{\partial x_i} \right) - \frac{2}{3} \left( \rho k + \mu \frac{\partial u_i}{\partial x_j} \right) \delta_{ij} \quad (3)$$

Where  $\mu_t$  is the turbulent viscosity, and  $k$  is the turbulent kinetic energy.

The standard  $k - \omega$  two-equation turbulence model was used to simulate the water penetration. And it has proven to be more suitable than the  $k - \varepsilon$  model used to describe the flow field of WAIM [15].

The heat exchange between the water and the melt was taken into consideration in the injection process, and the energy equation is,

$$\frac{\partial (\rho E)}{\partial t} + \frac{\partial}{\partial x_j} [u_i (\rho E + p)] = \frac{\partial}{\partial x_j} \left[ \lambda_{eff} \frac{\partial T}{\partial x_j} + u_i (\tau_{ij})_{eff} \right] \quad (4)$$

Where  $E$  is the fluid total energy,  $p$  the melt pressure,  $\lambda_{eff}$  the effective thermal conductivity coefficient, and  $(\tau_{ij})_{eff}$  the deviatoric stress tensor.

In WACIM, the shear stress is the main influencing factors of the melt flows in the mold cavity. Therefore, the elastic behavior of the melt was neglected, and the generalized Newtonian fluid constitutive model was adopted for WACIM simulation.

Water cools the inside of the melt directly, and the melt temperature in WACIM is low. In order to characterize the viscosity of the low temperature melt, the Cross-WLF viscosity model with seven parameters was used in the simulations.

Because the melt and the water are moving surface flows without mutual penetration between the adjacent phases, the VOF method was used to track the moving interfaces of the skin melt–inner melt and inner melt–water.

The physical properties were determined by the split-phase that existed in every control volume. For the skin–inner interface and the inner melt–water interface, the density, viscosity, and total energy were calculated as a volume fraction weighted average.

## 2.2 Boundary Conditions

The velocity inlet boundary condition was specified, the temperature was assumed to be uniform, and the volume fraction of the fluid beginning to be injected was defined as 1:

$$\mathbf{u} = \mathbf{u}_{inner}, T = T_{inner}, F_{inner} = 1 \quad t \geq t_{inner} \quad (5)$$

$$\mathbf{u} = \mathbf{u}_{water}, T = T_{water}, F_{water} = 1 \quad t \geq t_{water} \quad (6)$$

The pressure was specified as atmospheric pressure at the outlets. The no-slip boundary condition at the wall was specified, and the temperature at the wall was fixed.

## 2.3 Numerical Procedure

GAMBIT, a CFD special pre-processing software, was used to get a geometric model and mesh model. The numerical simulations were conducted with FLUENT, where the finite volume method was used to solve the conservation equations.

The solver was a 1st-order implicit unsteady formulation. In order to improve accuracy, the PISO algorithm was adopted to solve the pressure–velocity coupling equation for its applicability for unsteady flow, the moving interfaces were captured using the VOF method. For convergence and smoothness of solutions, the under-relaxation factors were all set to 0.25.

## 2.4 Molded Parts

Four typical non-circular cross-section tubes were selected for this study. These sections are shown in Figure 1. The cross-sections of A and B have four concave corners, while C has six concave corners and two convex corners, and D has two concave corners. The lengths of these tubes were 200 mm and the water gate was a cylinder with a diameter of 8 mm and a length of 10 mm. In a realistic mold, all edges of the cavity would be filleted with a radius of 2 mm; this has been omitted in these simulations. These four cavities were discretized with a mesh of quadrilaterals of 24,080, 37,779, 33,124 and 44,296, respectively.

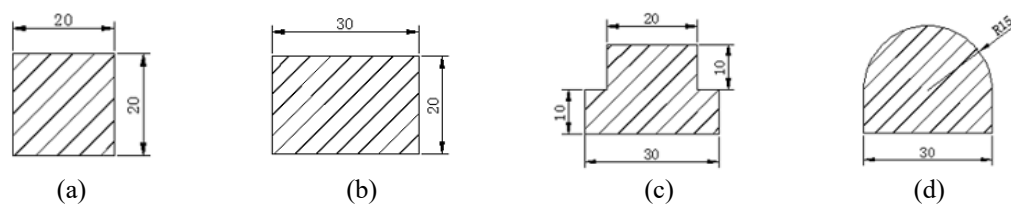


**Figure 1.** Cross-sections of the molded non-circular tubes.

For the reference simulation tests, the skin material was high density polyethylene (HDPE, Rigidex HM5420XP, BP Chemicals Corp.) and the inner material was polypropylene (PP, Globalene PC366, Taiwan PP Corp.). Their Cross–WLF viscosity model parameters were obtained from the MOLDFLOW material library and listed in Table 1.

**Table 1.** Cross–WLF model constants of the materials chosen for simulations.

	$\tau^*$ (Pa)	n (Pa)	D1 (Pa·s)	D2 (K)	D3 (K/Pa)	A1	$\bar{A}_2$ (K)
HDPE	5.73e+004	0.2837	1.71e+018	153.2	0	35.357	51.6
PP	24075	0.2921	2.02e+015	263.15	0	33.242	51.6

Table 2 shows the processing parameters used in the simulations.

**Table 2.** Processing parameters used in the simulations.

Parameters	Skin melt temp. (K)	Inner melt temp. (K)	Water temp. (K)	Water pressure (MPa)	Mold temp. (K)	Water delay time (s)
Value	483	473	300	6	320	3

### 3. Experiments

#### 3.1 Equipment Setup

The water assisted co-injection equipment was comprised of an injection molding machine, a water-injection controller, and a mold to form the test specimens. The molding machine was a 110-ton co-injection molding machine (FB-110C, FCS Group, Taiwan) with an external connection to the lab-developed water-injection unit. The water-injection unit consisted of a plunger water pump with a maximum pressure of 33 MPa, a pressure-regulating valve, a water injection pin, and a water tank. The moving of the water injection pin was driven by a pneumatic control system. The mold was able to accommodate interchangeable inserts to allow for flexibility in specimen geometry. In order to disconnect the part cavity and the overflow cavity, a pin was located at the overflow channel and controlled by a pneumatic control system as well. In FS-WACIM, the pin was drawn back such that the melt could be pushed into the overflow cavity, while in SS-WACIM, the pin was ejected out such that the overflow cavity was blocked from the part cavity.

#### 3.2 Materials and Processing

In the experiments, high density polyethylene (Grade DMDA-8008, Dushanzi Petrochemical Co., China) and polypropylene (Grade 1102K, Jinxi Petrochemical Co., China) were used as the skin material and the inner melt, respectively. In order to identify the interface between the skin and the inner melt, black and red colorants were added, respectively.

Table 3 lists the processing variables as well as the values used in the experiments.

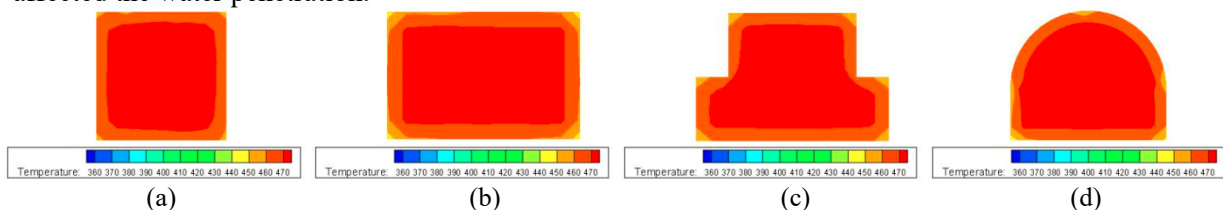
**Table 3.** Processing parameters in the experiment.

Parameters	Skin melt temp. (K)	Inner melt temp. (K)	Water temp. (K)	Water pressure (MPa)	Mold temp. (K)	Water delay time (s)	Hold packing time (s)
Value	483	473	300	6	320	3	60

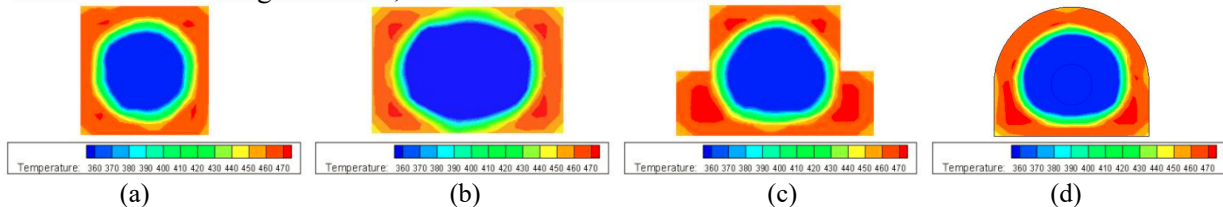
### 4. Results and Discussion

The results at locations of 40 mm and 150 mm from the water inlet were selected to investigate the inner melt and the water penetration interface changes at different positions, as well as before and after water injection.

The temperature distributions before water injection at the 40 mm location for the different cavities are shown in Figure 2. For cavities A, B, and D, the isotherms took the shape of the cross-sections. For cavity C, owing to the poor heat dissipation at the convex corners, the isotherms were close to the convex corners. The temperature distribution affected the viscosity distribution directly, which subsequently affected the water penetration.

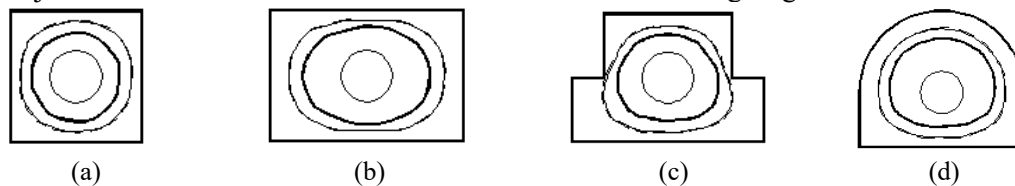
**Figure 2.** Temperature fields at the 40 mm location before water injection.

The temperature distributions at the end of the filling stage for WACIM at the 40 mm location for the different cavities are shown in Figure 3. As can be seen, the water penetrated the center of the cavities, where the temperature was high and the melt viscosity was low. The temperature near the water dropped sharply. The two methods of cooling—the inner water cooling the melt from the inside and the mold wall cooling the melt from the outside—resulted in the hottest areas being located near the concave corners. If the cooling is too fast, shrink voids will form in these areas.



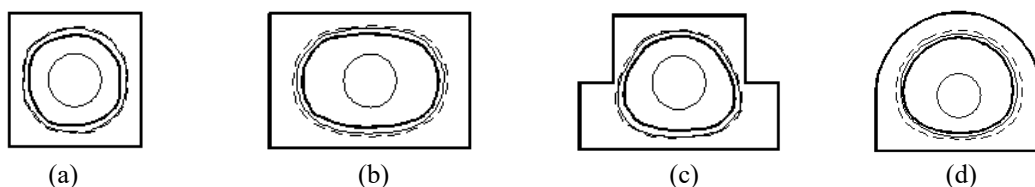
**Figure 3.** Temperature fields at the 40 mm location at the end of the filling process

Figure 4 shows the penetration cross-sections of the inner melt and the water at the 40 mm location. For cavity A, the penetration section of the inner melt was close to a circle shape, while the water was a circle in shape. For cavity B, the penetration section of the inner melt and the water were an elliptical shape. For cavity C, the penetration sections of the inner melt and the water were trapezoidal in shape. For cavity D, the penetration section of the inner melt and the water were close to a combination of half a circle and half an ellipse in shape. In general, the shapes of the water penetrations tended to be round. The simulation results showed that the penetration sections of the inner melt at the 40 mm location prior to water injection was almost the same as those at the end of the filling stage.



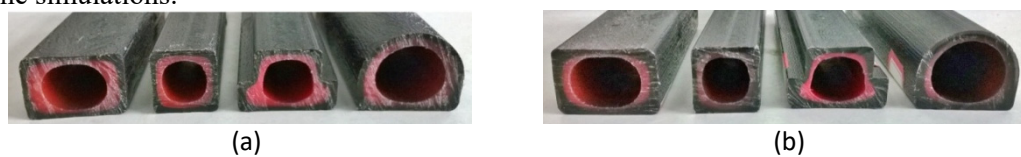
**Figure 4.** Penetration sections of the inner melt and the water at the 40 mm location: the thick line is for the water, the thin line is for the inner melt before water injection, and the dashed line is for the end of the filling process.

Figure 5 shows the penetration sections of the inner melt and the water at the 150 mm location. For all four cavity types, the penetration sections of the inner melt and the water were similar to those at the 40 mm location. However, it can be seen that the penetration sections of the inner melt at the 150 mm location for all four types of cavities were enlarged after water injection. The residual thicknesses of the inner melts were thinner than those at the 40 mm location. Lastly, the penetration sections of the water at the 150 mm location were bigger than those at the 40 mm location. This was because the pressure gradient in front of the water increased as the water penetrated, such that more inner melt could be pushed in the flow direction, leading to the increase of the penetration area of the water and the decrease of the residual wall thickness of the inner melt. As the water penetrated, the inner melt was pushed in the transverse direction by the higher pressure, such that the interface of skin-inner increased as well.



**Figure 5.** Penetration sections of the inner melt and the water at the 150 mm location: the thick line is for the water, the thin line is for the inner melt before water injection, and the dashed line is for the end of filling.

The experimental specimens were cut transverse at locations of 40 mm and 150 mm from the water inlet. The inner melt and the water penetration interfaces are shown in Figure 6. In order to compare the penetration interfaces at different locations conveniently, the interfaces were traced and combined together as shown in Figure 7. At the 40 mm location, the inner–outer melt interfaces in all of the specimens were similar to the cross-sections of the corresponding cavities, while at the 150 mm location, they were more round. The penetration areas of the inner melt at 40 mm were slightly larger than those at 150 mm. These results are in contrast to those of the simulations. This is because, in a real mold, the overflow channel in the cavities is small, while in the simulations, the ends of the cavities are used as outlet boundaries. The penetration sections of the water at the 150 mm location were larger than those at the 40 mm location. And the residual thicknesses of the inner melt at 150 mm were thinner than those at 40 mm. Aside from the exception stated above, the results of the experiments were in good agreement with those of the simulations.



**Figure 6.** Cross-sections of the specimens at the locations (a) 40 mm and (b) 150 mm from the water inlet.

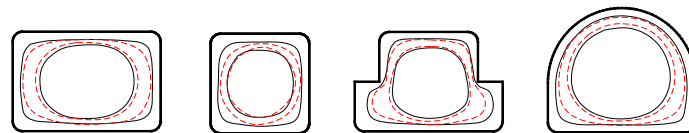


**Figure 7.** Penetration interfaces in the specimens: the solid black line is for the 40 mm location and the red dashed line is for the 150 mm location, the inner line is for the water–inner melt interface, and the outer line is for the inner–skin melt interface.

## 5. Conclusions

A three-dimensional model for WACIM was developed and the  $k - \omega$  turbulence model was adopted to deal with the turbulent flow of the water. Numerical simulations for the filling stage of WACIM parts with different cross-sections were carried out using the CFD method. In general, the results of the simulations corresponded with those of the experiments, which verified that the CFD model was excellent at handling the penetration of the inner melt and the water in WACIM. The cross-section shape of the cavity had a significant influence on the penetration section of the inner melt, while the shape of the water penetration section tended to be round. The shape of the penetration section of the water increased in the flow direction and the residual wall thicknesses of the inner melt downstream were thinner than those upstream.

## Acknowledgements

The authors would like to acknowledge the financial support of the National Nature Science Foundation of China (No. 51563010) and the Nature Science Foundation of Jiangxi Province (No. 20181BAB206014).

## References

- [1] Lang S and Parkinson M J 2005 *Plastics, Rubber and Composites* 34 (5-6) 232-5
- [2] Linse F, Giessauf J and Steinbichler G 2007 *Kunststoffe International* 11 68-70
- [3] Knights M 2002 *Plastics Technology* 48 (4) 42-7 .
- [4] Liu S J and Chen Y S 2003 *Polymer Engineering and Science* 43 (11) 1806-17
- [5] Park H P, Cha B S, Park S B, et al. 2014 *Advances in Materials Science and Engineering* <http://dx.doi.org/10.1155/2014/238251>

- [6] Seldén R 2000 Polymer Engineering and Science 40 (5) 1165-76
- [7] Kim N H and Isayev A I 2014 Polymer Engineering and Science DOI: 10.1002/pen.23871
- [8] Yan L 2007 Dissertation of Nanchang University China.
- [9] Kuang T Q and Deng Y 2013 China Plastics 27 (1) 106-10.
- [10] Zhang K, Kuang T Q, Liu H S and Zeng X S 2013 Polymer Materials Science and Engineering 29 (11) 178-82
- [11] Zhang K, Kuang T Q, Liu H S and Zeng X S 2013 Polymer Materials Science and Engineering 29 (6) 174-7.
- [12] Zhou G F, Chao F C and Zhang Y 2013 Engineering Plastics Application 41 (1) 47-9
- [13] Wu Y C, Chen K M and Liu S J 2006 Plastics, Rubber and Composites 35 (10) 425-31
- [14] Zhang Z Z, Zhou H, Gao Y A and Yang H Y 2010 Journal of Mechanical Engineering 46 (8) 140-6